Mem. S.A.It. Vol. 79, 1124

Memorie della

Disk-outflow connection and the molecular dusty torus

Moshe Elitzur

Physics & Astronomy Dept., University of Kentucky, Lexington, KY 40506-0055, USA
e-mail: moshe@pa.uky.edu

Abstract. Toroidal obscuration is a keystone of AGN unification. There is now direct evidence for the torus emission in infrared, and possibly water masers. Here I summarize the torus properties, its possible relation to the immediate molecular environment of the AGN and present some speculations on how it might evolve with the AGN luminosity.

Key words. dust, extinction – galaxies: active – galaxies: Seyfert – infrared: general – quasars: general – radiative transfer

1. Introduction

Although there are numerous classes of active galactic nuclei (AGN), a unified scheme has been emerging steadily (e.g., Antonucci, 1993; Urry & Padovani, 1995). The nuclear activity is powered by a supermassive ($\sim 10^6$–10^{10} $M_\odot$) black hole and its accretion disk. This central engine is surrounded by a dusty torus, which can be considered an acronym for Toroidal Obscuration Required by Unification Schemes: much of the observed diversity is simply explained as the result of viewing this axisymmetric geometry from different angles. Because of the anisotropic obscuration of the central region, sources viewed face-on are recognized as "type 1", those observed edge-on are "type 2". From basic considerations, Krolik & Begelman (1988) concluded that the obscuration is likely to consist of a large number of individually very optically thick dusty clouds.

2. Torus properties

2.1. Obscuration

There are clear indications that the optical depth at visual in the torus equatorial plane is at least $\tau_V \gtrsim 10$. If the dust abundance in the torus is similar to Galactic interstellar regions, the equatorial column density is at least $N_H \gtrsim 2{\times}10^{22}$ cm^{-2}.

The classification of AGN into types 1 and 2 is based on the extent to which the nuclear region is visible, therefore source statistics can determine the angular extent of the torus obscuration. In its standard formulation, the unification approach posits the viewing angle as the sole factor in determining the AGN type. This is indeed the case for a smooth-density torus that is optically thick within the angular width σ (figure 1, left sketch). If f_2 denotes the fraction of type 2 sources in the total population, then $f_2 = \sin\sigma$. From statistics of Seyfert galaxies Schmitt et al. (2001) find that $f_2 \simeq 70\%$. and deduce $\sigma \simeq 45°$. If H denotes the torus height at its outer radius R_o, this implies

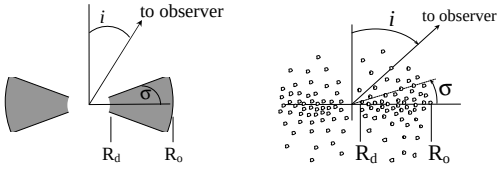

Fig. 1. AGN classification according to unified schemes. *Left*: In a smooth-density torus, the viewing angle (from the axis) $i = \frac{1}{2}\pi - \sigma$ separates between type 1 and type 2 viewing. *Right:* In a clumpy, soft-edge torus, the probability for direct viewing of the AGN decreases away from the axis, but is always finite.

$H/R_o \sim 1$. Taking account of the torus clumpiness modifies this relation fundamentally, as is evident from the right sketch in figure 1: the obscuration of the central engine becomes a viewing-angle dependent probability that depends on both the width of the cloud angular distribution and the number of clouds along the line of sight. In a Gaussian angular distribution with 5 clouds along radial rays in the equatorial plane, $f_2 = 70\%$ implies $\sigma = 33^\circ$ and $H/R_o \sim 0.7$ (Nenkova et al., 2008b). The clumpy nature of the obscuration also implies that AGN can occasionally flip between types 1 and 2, as observed (see Aretxaga et al., 1999, and references therein).

2.2. IR emission

An obscuring dusty torus should reradiate in the IR the fraction of nuclear luminosity it absorbs, and most AGNs do show significant IR emission. The top panel of figure 2 shows the composite type 1 spectra from a number of compilations. The optical/UV region shows the power law behavior expected from a hot disk emission. At $\lambda \gtrsim 1\mu$m, the SED shows the bump expected from dust emission. The bottom panel shows the same data after subtracting a power law fit through the short wavelengths in a crude attempt to remove the direct AGN component and mimic the SED from an equatorial viewing of these sources according to the unification scheme. Indeed, the AGN-subtracted SEDs resemble the observations of type 2 sources. Silicates reveal their presence in the dust through the 10 μm feature. The feature appears generally in emission in type 1 sources and in absorption in type 2 sources (Hao et al., 2007).

The torus dust emission has been resolved recently in 8–13 μm interferometry with the VLTI. The first torus was detected in NGC 1068 by Jaffe et al. (2004), the second in Circinus by Tristram et al. (2007). The latter observations show evidence for the long anticipated clumpy structure. The dust temperature distributions deduced from these observations indicate close proximity between hot (> 800 K) and much cooler (~ 200–300 K) dust. Such behavior is puzzling in the context of smooth-density calculations but is a natural consequence of clumpy models (Nenkova et al., 2008a).

2.3. Torus size

Obscuration statistics provide an estimate of the torus angular width $\sigma = \tan^{-1} H/R_o$ (fig. 1); the obscuration does not depend individually on either H or R_o, only on their ratio. To determine an actual size one must rely on the torus emission. The torus inner radius, R_d, is set by dust sublimation as

$$R_d \simeq 0.4\, L_{45} \text{ pc}, \quad (1)$$

where L_{45} is the bolometric luminosity in units of 10^{45} erg s^{-1}, and high-resolution IR observations trace the torus to an outer radius $R_o \sim 5$–$10\, R_d$; there is no compelling evidence that torus clouds beyond ~ 20–$30\, R_d$ need be considered (for details, see Nenkova et al., 2008b). A conservative upper bound on the torus outer radius is then $R_o \lesssim 12\, L_{45}^{1/2}$ pc.

2.4. Torus orientation and the host galaxy

Since the active region is a galactic nucleus, some obscuration can arise from the host galaxy. However, although galactic obscuration affects some individual sources, the strong orientation-dependent absorption cannot be generally attributed to the host galaxy because the AGN axis, as traced by the jet

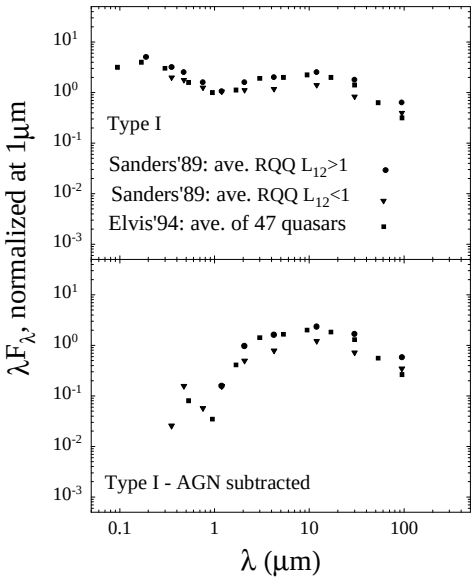

Fig. 2. SEDs of type 1 sources. Top: Average spectra from the indicated compilations. Bottom: The same SEDs after subtracting a power law fit through the short wavelengths ($\lesssim 1\mu$m). These AGN-subtracted SEDs are similar to those observed in type 2 sources.

position angle, is randomly oriented with respect to the galactic disk in Seyfert galaxies (Kinney et al., 2000) and the nuclear dust disk in radio galaxies (Schmitt et al., 2002). In addition, Guainazzi et al. (2001) find that heavily obscured AGN reside in a galactic environment that is as likely to be 'dust-poor' as 'dust-rich'.

3. NGC 1068—Case study of the molecular environment

NGC 1068 is the archetype Seyfert 2 galaxy and one of the most studied active nuclei. While the galaxy is oriented roughly face-on, its AGN torus is edge-on to within $\sim 5°$, as indicated by the geometry and kinematics of both water maser (Greenhill & Gwinn, 1997; Gallimore et al., 2001) and narrow-line emission (Crenshaw & Kraemer, 2000). The masers trace the disk to $\lesssim$ 1pc, inside the torus which is traced by IR to $\sim$ 2–3 pc (Jaffe et al., 2004). A nearly edge-on molecular structure is traced to distances much larger than the torus outer edge. Galliano et al. (2003) model the CO and H_2 emission from the central region with a clumpy molecular disk tilted roughly 15° from edge on. The disk has a radius of 140 pc and scale height of 20 pc, for $H/R \sim 0.15$. From CO velocity dispersions, Schinnerer et al. (2000) find the same $H/R \sim 0.15$ at $R \simeq 70$ pc. Thus, although resembling the putative torus, the detected molecular clouds are located in a thin disk-like structure, that does not meet the unification scheme requirement $H/R \sim 1$, outside the torus. The molecular disk orientation is much closer to the AGN than the host galaxy. Recent adaptive optics observations by Müller Sánchez et al. (2008) show evidence for molecular clumps in infall centered on the nucleus, on a scale of only ~ 10 pc. Imaging polarimetry at 10μm by Packham et al. (2007) shed some light on the continuity between the torus and the host galaxy's nuclear environment.

These observations suggest that the AGN in NGC 1068 might be at the center of a disk that extends beyond 100 pc, misaligned with the galactic disk. While this central disk has a warped structure, it maintains its orientation to within $\sim 15°$ and thickness (H/R) to within ~ 0.15. The disk outer regions are traced by molecular emission, the very inner regions ($\lesssim 10^3$ Schwarzchild radii) provide the direct accretion channel for the black hole. In between, the broad lines region (BLR) and torus clouds form structures much thicker than the disk.

4. The BLR/TOR continuity

Two different types of observations show that the torus is a smooth continuation of the broad lines region, not a separate entity. IR reverberation observations by Suganuma et al. (2006) measure the time lag of the dust radiative response to temporal variations of the AGN luminosity, determining the torus innermost radius. Their results show that this radius scales with luminosity as $L^{1/2}$ and is uncorrelated with the black hole mass, demonstrating that the torus inner boundary is controlled by dust sublimation (eq. 1), not by dynamical processes. Moreover, in each AGN for which both

data exist, the IR time lag is the upper bound on all time lags measured in the broad lines, a relation verified over a range of 10^6 in luminosity. This finding shows that the BLR extends outward all the way to the inner boundary of the dusty torus, validating the Netzer & Laor (1993) proposal that the BLR size is bounded by dust sublimation. The other evidence is the finding by Risaliti et al. (2002) that the X-ray absorbing columns in Seyfert 2 galaxies display time variations caused by cloud transit across the line of sight. Most variations come from clouds that are dust free because of their proximity (< 0.1 pc) to the AGN, but some involve dusty clouds at a few pc. Other than the different time scales for variability, there is no discernible difference between the dust-free and dusty X-ray absorbing clouds, nor are there any gaps in the distribution. These observations show that the X-ray absorption, broad line emission and dust obscuration and reprocessing are produced by a single, continuous distribution of clouds. The different radiative signatures merely reflect the change in cloud composition across the dust sublimation radius $R_{\rm d}$. The inner clouds are dust free. Their gas is directly exposed to the AGN ionizing continuum, therefore it is atomic and ionized, producing the broad emission lines. The outer clouds are dusty, therefore their gas is shielded from the ionizing radiation, and the atomic line emission is quenched. Instead, these clouds are molecular and dusty, obscuring the optical/UV emission from the inner regions and emitting IR. Thus the BLR occupies $r < R_{\rm d}$ while the torus is simply the $r > R_{\rm d}$ region. Both regions absorb X-rays, but because most of the clouds along each radial ray reside in its BLR segment, that is where the bulk of the X-ray obscuration is produced. Since the unification torus is just the outer portion of the cloud distribution and not an independent structure, it is appropriate to rename it the TOR for Toroidal Obscuration Region.

4.1. Outflow origin for the BLR/TOR?

The merger of the BLR ionized clouds and TOR dusty clouds into a single population fits naturally into a scenario first proposed by Emmering et al. (1992), involving the outflow of clouds embedded in a hydromagnetic disk wind. The clouds are accelerated by the system rotation along magnetic field lines anchored in the disk, as first described by Blandford & Payne (1982). In this approach the TOR is that region in the wind which happens to provide the required toroidal obscuration because the clouds there are dusty and optically thick. The mounting evidence for cloud outflow with the geometry and kinematics of disk winds (e.g., Elvis, 2004; Gallagher & Everett, 2007) is in accord with the outflow paradigm.

The wind scenario for the AGN toroidal obscuration unifies naturally the different components of the system (Elitzur & Shlosman, 2006). The AGN accretion disk appears to be fed by a midplane influx of cold, clumpy material (Shlosman et al., 1990, and references therein). Approaching the center, conditions for developing hydromagnetically- or radiatively-driven winds above this equatorial inflow become more favorable. The disk-wind rotating geometry provides a natural channel for angular momentum outflow from the disk (Blandford & Payne, 1982) and is found on many spatial scales, from protostars to AGN. The composition along each streamline reflects the origin of the outflow material at the disk surface. The disk outer regions are dusty and molecular, as observed in water masers in some edge-on cases (Greenhill, 2005), and clouds uplifted from these outer regions feed the TOR. Such clouds have been detected in water maser observations of Circinus and NGC 3079. The Circinus Seyfert 2 core provides the best glimpse of the AGN dusty/molecular component. Water masers trace both a Keplerian disk and a disk outflow (Greenhill et al., 2003). Dust emission at 8–13μm shows a disk embedded in a slightly cooler and larger, geometrically thick torus (Tristram et al., 2007). The dusty disk coincides with the maser disk in both orientation and size. The outflow masers trace only parts of the torus. The lack of full coverage can be attributed to the selectivity of maser operation—strong emission requires both pump action to invert the maser molecules in individual clouds and coinci-

dence along the line of sight in both position and velocity of two maser clouds (Kartje et al., 1999). In NGC 3079, four maser features were found significantly out of the plane of the maser-traced disk yet their line-of-sight velocities reflect the velocity of the most proximate side of the disk. Kondratko et al. (2005) note that this can be explained if, as proposed by Kartje et al. (1999), maser clouds rise to high latitudes above the rotating structure while still maintaining, to some degree, the rotational velocity imprinted by the parent disk. Because the detected maser emission involves cloud-cloud amplification that requires precise alignment in both position and velocity along the line-of-sight, the discovery of four high-latitude maser features implies the existence of many more such clouds partaking in the outflow in this source. Moving inward from the dusty/molecular regions, at some smaller radius the dust is destroyed and the disk composition switches to atomic and ionized, producing a double-peak signature in some emission line profiles (Eracleous, 2004). The outflow from the atomic/ionized inner region feeds the BLR and produces many atomic line signatures, including evidence for the disk wind geometry (Hall et al., 2003).

The outflow paradigm requires only the accretion disk and the clumpy outflow it generates. Cloud radial distance from the AGN center and vertical height above the accretion disk explain the rich variety of observed radiative phenomena. In both the inner and outer outflow regions, as the clouds rise and move away from the disk they expand and lose their column density, limiting the vertical scope of X-ray absorption, broad line emission and dust obscuration and emission. The result is a toroidal geometry for both the BLR and the TOR. With further rise and expansion, the density decreases so the ionization parameter increases, turning the clouds into members of the warm absorber population. Similar considerations can explain the broad absorption lines observed in some quasars (BAL/QSO; Gallagher & Everett, 2007).

4.2. TOR cloud properties

From IR modeling, the optical depth of individual clouds should lie in the range $\tau_V \sim 30$–100 (Nenkova et al., 2008b). Assuming standard dust-to-gas ratio, the cloud column density is $N_H \sim 10^{22}$–10^{23} cm^{-2}. The cloud density can be constrained separately because it must be able to withstand the black-hole tidal shearing effect. Resistance to tidal shearing sets a lower limit on the density of the cloud n_{cl}, leading to upper limits on its size R_{cl} and mass M_{cl} as follows (Elitzur & Shlosman, 2006):

$$\begin{aligned} n_{cl} &\gtrsim 10^7 \frac{M_{\bullet 7}}{r_{pc}^3}\ \mathrm{cm}^{-3}, \\ R_{cl} &\lesssim 10^{16} \frac{N_{H,23} r_{pc}^3}{M_{\bullet 7}}\ \mathrm{cm}, \\ M_{cl} &\lesssim 7{\times}10^{-3} N_{H,23} R_{16}^2\ M_\odot \end{aligned} \tag{2}$$

In these expressions r_{pc} is the distance in pc from a black-hole with mass $M_{\bullet 7}$ in $10^7\ M_\odot$, $n_7 = n_{cl}/(10^7\ \mathrm{cm}^{-3})$, $N_{H,23} = N_H/(10^{23}\ \mathrm{cm}^{-2})$ and $R_{16} = R_{cl}/(10^{16}\ \mathrm{cm})$. The resistance to tidal shearing does not guarantee confinement against the dispersive force of internal pressure. Self-gravity cannot confine these clouds because their low masses provide gravitational confinement only against internal motions with velocities $\lesssim 0.1$ km s^{-1}. A corollary is that these clouds cannot collapse gravitationally to form stars. While self-gravity cannot hold a cloud together against dispersal, an external magnetic field $B \sim 1.5\,\sigma_5 n_7^{1/2}$ mG would suffice if the internal velocity dispersion is $\sigma_5{\times}1$ km s^{-1}. Clouds with these very same properties can explain the masers detected in Circinus and NGC 3079, adding support to the suggestion that the outflow water masers are yet another manifestation of the dusty, molecular clouds that make up the torus region of the disk-wind. Proper motion measurements and comparisons of the disk and outflow masers offer a most promising means to probe the structure and motion of TOR clouds.

The Resistance to tidal shearing dictates that the density inside the cloud increase as $1/r^3$ as it gets closer to the central black-hole (eq. 2). A cloud of a given density can exist only beyond a certain radial distance; only

denser clouds can survive at smaller radii, leading to a radially stratified structure. Similarly, the Keplerian velocity increases as $1/r^{1/2}$ as the black-hole is approached. Typical BLR cloud densities and velocities occur at $r \sim 10^{16}$–10^{17} cm. It is possible that the BLR inner boundary occurs where the clouds can no longer overcome the black-hole tidal shearing.

4.3. The AGN low-luminosity end

The total TOR mass outflow rate, calculated using the properties of single clouds listed in eq. 2, exceeds its accretion rate when $L \lesssim 10^{42}$ erg s^{-1}. Therefore, a key prediction of the wind scenario is that the torus disappears at low bolometric luminosities because mass accretion can no longer sustain the required cloud outflow rate, i.e., the large column densities (Elitzur & Shlosman, 2006). Observations seem to corroborate this prediction. In an HST study of a complete sample of low-luminosity ($\lesssim 10^{42}$ erg s^{-1}) FR I radio galaxies, Chiaberge et al. (1999) detected the compact core in 85% of sources. Since the radio selection is unbiased with respect to the AGN orientation, FR I sources should contain similar numbers of type 1 and type 2 objects, and Chiaberge et al suggested that the high detection rate of the central compact core implies the absence of an obscuring torus. This suggestion was corroborated by Whysong & Antonucci (2004) who demonstrated the absence of a dusty torus in M87, one of the sources in the FR I sample, by placing stringent limits on its thermal IR emission. Observations by Perlman et al. (2007) further solidified this conclusion. The behavior displayed by M87 appears to be common in FR I sources. Van der Wolk et al (private communication) performed high resolution 12 μm imaging observations of the nuclei of 27 radio galaxies with the VISIR instrument on the VLT. These observations provide strong confirmation of the torus disappearance in FR I sources. They show that all the FR I objects in the sample lack dusty torus thermal emission, although they have non-thermal nuclei. Thermal dust emission was detected in about half the FR II nuclei, which generally have higher luminosities. In contrast, in almost all broad line radio galaxies in the sample the observations detected the thermal nucleus. Significantly, Ogle et al. (2007) find that most FR I and half of FR II sources have $L/L_{\rm Edd} < 3 \cdot 10^{-3}$, while all sources with broad Balmer lines have $L/L_{\rm Edd} > 3 \cdot 10^{-3}$ (note that $L_{\rm Edd} = 10^{45} M_{\bullet 7}$ erg s^{-1}).

The AGNs known as LINERs provide additional evidence for the torus disappearance. Maoz et al. (2005) conducted UV monitoring of LINERs with $L \lesssim 10^{42}$ erg s^{-1} and detected variability in most of them. This demonstrates that the AGN makes a significant contribution to the UV radiation in each of the monitored sources and that it is relatively unobscured in all the observed LINERs, which included both type 1 and type 2. Furthermore, the histograms of UV colors of the type 1 and 2 LINERs show an overlap between the two populations, with the difference between the histogram peaks corresponding to dust obscuration in the type 2 objects of only ~ 1 magnitude in the R band. Such toroidal obscuration is minute in comparison with the torus obscuration in higher luminosity AGN. The predicted torus disappearance at low L does not imply that the cloud component of the disk wind is abruptly extinguished, only that its outflow rate is less than required by the IR emission observed in quasars and high-luminosity Seyferts. When the outflow drops below these "standard" torus values, the outflow still provides toroidal obscuration as long as its column exceeds $\sim 10^{21}$ cm^{-2}. Indeed, Maoz et al find that some LINERs do have obscuration, but much smaller than "standard". Line transmission through a low-obscuration torus might also explain the low polarizations of broad Hα lines observed by Barth et al. (1999) in some low luminosity systems.

If the toroidal obscuration were the only component removed from the system, all low luminosity AGN would become type 1 sources. In fact, among the LINERs monitored and found to be variable by Maoz et al there were both sources with broad Hα wings (type 1) and those without (type 2). Since all objects are relatively unobscured, the broad line component is truly missing in the type 2 sources

in this sample. Similarly, Panessa & Bassani (2002) note that the BLR is weak or absent in low luminosity AGN, and Laor (2003) presents arguments that some "true" type 2 sources, i.e., having no obscured BLR, do exist among AGNs with $L \lesssim 10^{42}\,\mathrm{erg\,s^{-1}}$. The absence of broad lines in these sources cannot be attributed to toroidal obscuration because their X-ray emission is largely unobscured. These findings have a simple explanation if when L decreases further beyond the disappearance of the TOR outflow, the suppression of mass outflow spreads radially inward from the disk's dusty, molecular region into its atomic, ionized zone. Then the torus disappearance, i.e., removal of the toroidal obscuration by the dusty wind, would be followed by a diminished outflow from the inner ionized zone and disappearance of the BLR at some lower luminosity. Indeed, a recent review by Ho (2008) presents extensive observational evidence for the disappearance of the torus and the BLR in low luminosity AGN. Such an inward progression of the outflow turnoff as the accretion rate decreases can be expected naturally in the context of disk winds because mass outflow increases with the disk area. A diminished supply of accreted mass may suffice to support an outflow from the inner parts of the disk but not from the larger area of its outer regions. And with further decrease in inflow rate, even the smaller inner area cannot sustain the disk outflow. Since the accreted mass cannot be channeled in full into the central black hole, the system must find another channel for release of the excess accreted mass, and the only one remaining is the radio jets. Indeed, Ho (2002) finds that the AGN radio loudness $\mathcal{R} = L_{\rm radio}/L_{\rm opt}$ is *inversely* correlated with the mass accretion rate $L/L_{\rm Edd}$. This finding is supported by Sikora et al. (2007), who have greatly expanded this correlation and found an intriguing result: $\mathcal{R}$ indeed increases inversely with $L/L_{\rm Edd}$, but only so long as $L/L_{\rm Edd}$ remains $\gtrsim 10^{-3}$. At smaller accretion rates, which include all FR I radio galaxies, the radio loudness saturates and remains constant at $\mathcal{R} \sim 10^4$. This is precisely the expected behavior if as the outflow diminishes, the jets are fed an increasingly larger fraction of the accreted mass and finally, once the outflow is extinguished, all the inflowing material not funneled into the black hole is channeled into the jets, whose feeding thus saturates at a high conversion efficiency of accreted mass. It is important to note that radio loudness reflects the relative contribution of radio to the overall radiative emission; a source can be radio loud even at a low level of radio emission if its overall luminosity is small, and vice versa.

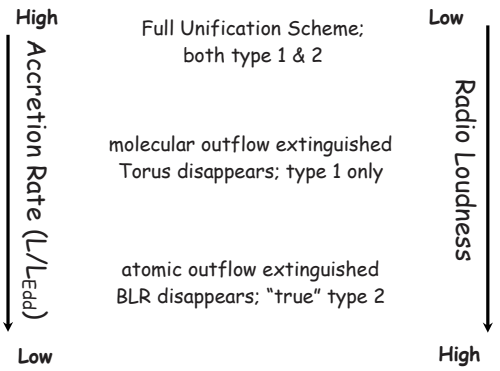

Fig. 3. Conjectured scheme for AGN evolution with decreasing accretion rate.

The evolutionary scheme just outlines is sketched in figure 3. A similar anti-correlation between radio loudness and accretion rate exists also in X-ray binaries. These sources display switches between radio quiet states of high X-ray emission and radio loud states with low X-ray emission (**?**). While in X-ray binaries this behavior can be followed with time in a given source, in AGN it is only manifested statistically. Comparative studies of AGN and X-ray binaries seem to be a most useful avenue to pursue.

Acknowledgements. Partial support by NSF and NASA is gratefully acknowledged.

References

Antonucci, R. 1993, ARA&A, 31, 473
Aretxaga, I., Joguet, B., Kunth, D., Melnick, J., & Terlevich, R. J. 1999, ApJ, 519, L123
Barth, A. J., Filippenko, A. V., & Moran, E. C. 1999, ApJ, 525, 673

Blandford, R. D. & Payne, D. G. 1982, MNRAS, 199, 883
Chiaberge, M., Capetti, A., & Celotti, A. 1999, A&A, 349, 77
Crenshaw, D. M. & Kraemer, S. B. 2000, ApJ, 532, L101
Elitzur, M. & Shlosman, I. 2006, ApJ, 648, L101
Elvis, M. 2004, in ASP Conf. Ser. 311: AGN Physics with the Sloan Digital Sky Survey, ed. G. T. Richards & P. B. Hall, 109
Emmering, R. T., Blandford, R. D., & Shlosman, I. 1992, ApJ, 385, 460
Eracleous, M. 2004, in ASP Conf. Ser. 311: AGN Physics with the Sloan Digital Sky Survey, ed. G. T. Richards & P. B. Hall, 183
Fender, R. P., Belloni, T. M., & Gallo, E. 2004, MNRAS, 355, 1105
Gallagher, S. C. & Everett, J. E. 2007, in ASP Conf. Ser. 373: The Central Engine of Active Galactic Nuclei, ed. L. C. Ho & J.-M. Wang, 305–314
Galliano, E., Alloin, D., Granato, G. L., & Villar-Martín, M. 2003, A&A, 412, 615
Gallimore, J. F., Henkel, C., Baum, S. A., et al. 2001, ApJ, 556, 694
Greenhill, L. J. 2005, in ASP Conf. Ser. 340: Future Directions in High Resolution Astronomy, ed. J. Romney & M. Reid, 203
Greenhill, L. J., Booth, R. S., Ellingsen, S. P., et al. 2003, ApJ, 590, 162
Greenhill, L. J. & Gwinn, C. R. 1997, Ap&SS, 248, 261
Guainazzi, M., Fiore, F., Matt, G., & Perola, G. C. 2001, MNRAS, 327, 323
Hall, P. B., Hutsemékers, D., Anderson, S. F., et al. 2003, ApJ, 593, 189
Hao, L., Weedman, D. W., Spoon, H. W. W., et al. 2007, ApJ, 655, L77
Ho, L. C. 2002, ApJ, 564, 120
Jaffe, W., Meisenheimer, K., Röttgering, H. J. A., et al. 2004, Nature, 429, 47
Kartje, J. F., Königl, A., & Elitzur, M. 1999, ApJ, 513, 180
Kinney, A. L., Schmitt, H. R., Clarke, C. J., et al. 2000, ApJ, 537, 152
Kondratko, P. T., Greenhill, L. J., & Moran, J. M. 2005, ApJ, 618, 618
Krolik, J. H. & Begelman, M. C. 1988, ApJ, 329, 702
Laor, A. 2003, ApJ, 590, 86
Maoz, D., Nagar, N. M., Falcke, H., & Wilson, A. S. 2005, ApJ, 625, 699
Müller Sánchez, F., Davies, R. I., Genzel, R., et al. 2008, in RMxAC vol 32, 109–111
Nenkova, M., Sirocky, M. M., Ivezić, Ž., & Elitzur, M. 2008a, ApJ, in press (arXiv:0806.0511)
Nenkova, M., Sirocky, M. M., Nikutta, R., Ivezić, Ž., & Elitzur, M. 2008b, ApJ, in press (arXiv:0806.0512)
Netzer, H. & Laor, A. 1993, ApJ, 404, L51
Ogle, P. M., Antonucci, R. R. J., & Whysong, D. 2007, in ASP Conf. Ser. 373: The Central Engine of Active Galactic Nuclei, ed. L. C. Ho & J.-M. Wang, 578–581
Packham, C., Young, S., Fisher, S., et al. 2007, ApJ, 661, L29
Panessa, F. & Bassani, L. 2002, A&A, 394, 435
Perlman, E. S., Mason, R. E., Packham, C., et al. 2007, ApJ, 663, 808
Risaliti, G., Elvis, M., & Nicastro, F. 2002, ApJ, 571, 234
Schinnerer, E., Eckart, A., Tacconi, L. J., Genzel, R., & Downes, D. 2000, ApJ, 533, 850
Schmitt, H. R., Antonucci, R. R. J., Ulvestad, J. S., et al. 2001, ApJ, 555, 663
Schmitt, H. R., Pringle, J. E., Clarke, C. J., & Kinney, A. L. 2002, ApJ, 575, 150
Shlosman, I., Begelman, M. C., & Frank, J. 1990, Nature, 345, 679
Sikora, M., Stawarz, Ł., & Lasota, J.-P. 2007, ApJ, 658, 815
Suganuma, M., Yoshii, Y., Kobayashi, Y., et al. 2006, ApJ, 639, 46
Tristram, K. R. W., Meisenheimer, K., Jaffe, W., et al. 2007, A&A, 474, 837
Urry, C. M. & Padovani, P. 1995, PASP, 107, 803
Whysong, D. & Antonucci, R. 2004, ApJ, 602, 116